(Fig. 4, A and B). In addition, $KL^{-/-}$ $IRS\text{-}1^{+/-}$ mice ameliorated many age-related pathologies typical of $KL^{-/-}$ mice, including arteriosclerosis, ectopic calcification, skin atrophy, pulmonary emphysema, and hypogonadism (Fig. 4, C to N). Heterozygosity of IRS-1 alone ($KL^{+/+}$ $IRS\text{-}1^{+/-}$ littermates) appears to have no effect on survival and the age-progressive degeneration when compared with those factors in wild-type littermates during these experiments (*9*).

Conclusion. We previously reported that a defect in *Klotho* gene expression leads to a syndrome that may resemble premature aging (*1*). Here, we show that overexpression of *Klotho* can extend life span, and we suggest that *Klotho* functions as an aging suppressor gene in mammals. We found that the extracellular domain of Klotho protein circulates in the blood and binds to a putative cell-surface receptor. Klotho has marked effects on insulin physiology, apparently because it suppresses tyrosine phosphorylation of insulin and IGF1 receptors, which results in reduced activity of IRS proteins and their association with PI3-kinase, thereby inhibiting insulin and IGF1 signaling. Extended life span upon negative regulation of insulin and IGF1 signaling is an evolutionarily conserved mechanism to suppress aging (*28*). Klotho appears to be a peptide hormone to modulate such signaling and thereby mediate insulin metabolism and aging.

References and Notes

1. M. Kuro-o *et al.*, *Nature* **390**, 45 (1997).
2. Y. Takahashi, M. Kuro-o, F. Ishikawa, *Proc. Natl. Acad. Sci. U.S.A.* **97**, 12407 (2000).
3. D. E. Arking *et al.*, *Proc. Natl. Acad. Sci. U.S.A.* **99**, 856 (2002).
4. D. E. Arking *et al.*, *Am. J. Hum. Genet.* **72**, 1154 (2003).
5. N. Ogata *et al.*, *Bone* **31**, 37 (2002).
6. K. Kawano *et al.*, *J. Bone Miner. Res.* **17**, 1744 (2002).
7. Y. Yamada, F. Ando, N. Niino, H. Shimokata, *J. Mol. Med.* **83**, 50 (2005).
8. D. E. Arking, G. Atzmon, A. Arking, N. Barzilai, H. C. Dietz, *Circ. Res.* **96**, 412 (2005).
9. M. Kuro-o *et al.*, data not shown.
10. F. Grabnitz, M. Seiss, K. P. Rucknagel, W. L. Staudenbauer, *Eur. J. Biochem.* **200**, 301 (1991).
11. R. Weindruch, R. L. Walford, S. Fligiel, D. Guthrie, *J. Nutr.* **116**, 641 (1986).
12. H. M. Brown-Borg, K. E. Borg, C. J. Meliska, A. Bartke, *Nature* **384**, 33 (1996).
13. R. A. Miller, *Sci. Aging Knowledge Environ.* **2001**, vp6 (2001).
14. G. C. Williams, *Evol. Int. J. Org. Evol.* **11**, 398 (1957).
15. C. Kenyon, J. Chang, E. Gensch, A. Rudner, R. Tabtiang, *Nature* **366**, 461 (1993).
16. J. Z. Morris, H. A. Tissenbaum, G. Ruvkun, *Nature* **382**, 536 (1996).
17. M. Tatar *et al.*, *Science* **292**, 107 (2001).
18. D. J. Clancy *et al.*, *Science* **292**, 104 (2001).
19. M. Holzenberger *et al.*, *Nature* **421**, 182 (2003).
20. M. Bluher, B. B. Kahn, C. R. Kahn, *Science* **299**, 572 (2003).
21. C. Kenyon, *Cell* **120**, 449 (2005).
22. T. Utsugi *et al.*, *Metabolism* **49**, 1118 (2000).
23. A. E. Halseth, D. P. Bracy, D. H. Wasserman, *Am. J. Physiol.* **276**, E70 (1999).
24. A. Imura *et al.*, *FEBS Lett.* **565**, 143 (2004).
25. A. R. Saltiel, C. R. Kahn, *Nature* **414**, 799 (2001).
26. D. LeRoith, C. T. Roberts Jr., *Cancer Lett.* **195**, 127 (2003).
27. E. Araki *et al.*, *Nature* **372**, 186 (1994).
28. M. Tatar, A. Bartke, A. Antebi, *Science* **299**, 1346 (2003).

29. We thank D. H. Wasserman and Vanderbilt Mouse Metabolic Phenotyping Center for physiological analysis of the mice; R. L. Dobbins for hyperinsulinemic euglycemic clamp experiments; J. A. Richardson and Molecular Pathology Core Facility at UT Southwestern for histological analysis; D. W. Russell at UT Southwestern for Klotho receptor identification; R. Komuro and H. Kuriyama at UT Southwestern for insulin and IGF1 signaling analysis; Genentech for providing IGF1; H. Masuda, T. Suga, R. Nagai, A. T. Dang, R. Shamlou, P. Bezzera, T. Reed, C. Iucu, W. Lai for earlier contributions and supports to this study; and E. C. Friedberg, M. S. Brown, and K. A. Wharton Jr. at UT Southwestern for critical reading of the manuscript. This work was supported in part by grants from Endowed Scholar Program at UT Southwestern (M.K.), Pew Scholars Program in Biomedical Science (M.K.), Eisai Research Fund (M.K.), High-Impact/High-Risk Research Program at UT Southwestern (M.K.), and NIH (R01AG19712 to M.K. and R01AG25326 to M.K. and K.P.R.). J.H. is supported by the NIH, the Perot Family Foundation, and the Humboldt Foundation.

Supporting Online Material
www.sciencemag.org/cgi/content/full/1112766/DC1
Materials and Methods
Figs. S1 to S7
Table S1
References

25 March 2005; accepted 4 August 2005
Published online 25 August 2005;
10.1126/science.1112766
Include this information when citing this paper.

REPORTS

Bright X-ray Flares in Gamma-Ray Burst Afterglows

D. N. Burrows,[1]* P. Romano,[2] A. Falcone,[1] S. Kobayashi,[1,3] B. Zhang,[4] A. Moretti,[2] P. T. O'Brien,[5] M. R. Goad,[5] S. Campana,[2] K. L. Page,[5] L. Angelini,[6,7] S. Barthelmy,[6] A. P. Beardmore,[5] M. Capalbi,[8] G. Chincarini,[2,9] J. Cummings,[6] G. Cusumano,[10] D. Fox,[11] P. Giommi,[8] J. E. Hill,[1] J. A. Kennea,[1] H. Krimm,[6] V. Mangano,[10] F. Marshall,[6] P. Mészáros,[1] D. C. Morris,[1] J. A. Nousek,[1] J. P. Osborne,[5] C. Pagani,[1,2] M. Perri,[8] G. Tagliaferri,[2] A. A. Wells,[5] S. Woosley,[12] N. Gehrels[6]

Gamma-ray burst (GRB) afterglows have provided important clues to the nature of these massive explosive events, providing direct information on the nearby environment and indirect information on the central engine that powers the burst. We report the discovery of two bright x-ray flares in GRB afterglows, including a giant flare comparable in total energy to the burst itself, each peaking minutes after the burst. These strong, rapid x-ray flares imply that the central engines of the bursts have long periods of activity, with strong internal shocks continuing for hundreds of seconds after the gamma-ray emission has ended.

Gamma-ray bursts (GRBs) are the most powerful explosions since the Big Bang, with typical energies around 10^{51} ergs. Long GRBs (duration > 2 s) are thought to signal the creation of black holes by the collapse of massive stars (*1–4*). The detected signals from the resulting highly relativistic fireballs consist of prompt gamma-ray emission (from internal shocks in the fireball) lasting for several seconds to minutes, followed by afterglow emission (from external shocks as the fireball encounters surrounding material) covering a broad range of frequencies from radio through x-rays (*5–7*). Because of the time needed to accurately determine the GRB position, most afterglow

[1]Department of Astronomy and Astrophysics, 525 Davey Lab, Pennsylvania State University, University Park, PA 16802, USA. [2]Istituto Nazionale di Astrofisica (INAF)–Osservatorio Astronomico di Brera, Via Bianchi 46, 23807 Merate, Italy. [3]Center for Gravitational Wave Physics, 104 Davey Lab, Pennsylvania State University, University Park, PA 16802, USA. [4]Department of Physics, University of Nevada, Box 454002, Las Vegas, NV 89154–4002, USA. [5]Department of Physics and Astronomy, University of Leicester, University Road, Leicester LE1 7RH, UK. [6]NASA/Goddard Space Flight Center, Greenbelt, MD 20771, USA. [7]Department of Physics and Astronomy, Johns Hopkins University, 3400 North Charles Street, Baltimore, MD 21218, USA. [8]Agenzia Spaziale Italiana Science Data Center, Via Galileo Galilei, 00044 Frascati, Italy. [9]Dipartimento di Fisica, Università degli studi di Milano-Bicocca, Piazza delle Scienze 3, 20126 Milan, Italy. [10]INAF–Istituto di Astrofisica Spaziale e Fisica Cosmica Sezione di Palermo, Via Ugo La Malfa 153, 90146 Palermo, Italy. [11]Department of Astronomy, California Institute of Technology, MS 105-24, Pasadena, CA, 91125, USA. [12]Department of Astronomy and Astrophysics, University of California, Santa Cruz, CA 95064, USA.

*To whom correspondence should be addressed. E-mail: burrows@astro.psu.edu

measurements have been made hours after the burst, and little is known about the characteristics of afterglows in the minutes following a burst, when the afterglow emission is actively responding to inhomogeneities in both the fireball and the circumburst environment.

The Swift (*8*) X-ray Telescope (XRT) (*9*) provides unique x-ray observations of young GRB and x-ray flash (XRF) afterglows, beginning in the first few minutes after the burst. (Here, we use the terms "burst" and "prompt emission" to refer to the burst seen in hard x-rays and gamma rays, and we use the term "afterglow" to refer to the soft x-ray, optical, and radio emission seen after the end of the detectable hard x-ray prompt emission.) Between 23 December 2004 and 5 May 2005, the XRT observed 13 afterglows within 200 s of the onset of GRBs discovered by the Swift Burst Alert Telescope (BAT) (*10*). In most cases, the XRT found a bright, monotonically decaying afterglow (*11*–*14*). In contrast, the afterglows of both XRF 050406 and GRB 050502B (*15*) were a factor of 10 to 1000 times fainter than previous XRT-detected afterglows at $T + 100$ s but brightened rapidly several minutes later before decaying back to their preflare fluxes (Fig. 1). The afterglow of XRF 050406 brightened by a factor of 6 between 150 and 213 s postburst and is similar to x-ray flares observed in a few previous cases (*16*). GRB 050502B is qualitatively different, with a giant flare that brightened by a factor of ~500 to a peak at $T + 740$ s. This flare contained roughly as much energy ($\sim 9 \times 10^{-7}$ ergs cm^{-2}, 0.3 to 10 keV) as the prompt emission observed by the BAT (8×10^{-7} ergs cm^{-2}, 15 to 350 keV), something never before seen and quite unexpected.

The rise and fall of the flare in XRF 050406 are both very steep. Following standard practice, we characterized the x-ray afterglow decays as power-laws with the x-ray flux varying as $F_x \propto t^{\alpha}$, where t is the time since GRB onset. Using this same form to describe the x-ray flare, we found $\alpha = +4.9 \pm 0.3$ during the rising portion and $\alpha = -5.7 \pm 0.6$ during the decay, with $\delta t/t_{peak} \sim 0.3$ and 0.6 for the rise and fall times, respectively. (The flare slopes are more symmetrical if the underlying power-law afterglow decay is subtracted.) Such large slopes cannot be explained by external forward shocks, in which the radiation physics implies a slower decay, with the decay time δt comparable to the postshock time t (*17*). The shape of the flare is reminiscent of that expected for an external reverse shock, created in the outflow when the forward shock is slowed substantially by interaction with an external medium. However, reverse shocks are expected to be far less steep and should be seen in the optical, not the x-ray, band. Synchrotron self-Compton (SSC) models may be able to produce x-ray emission from a reverse shock, but only for carefully balanced conditions (*18*). A far more natural explanation for this flare is continuation of strong internal shocks to a time of at least $T + 213$ s.

The flare in GRB 050502B is slower, with $\delta t_{decay}/t \sim 1$, but the sharp spike at $T + 740$ s (seen in the hard band in Fig. 2B) argues against an external shock mechanism (*17*). If produced by internal shocks, energy production by the central engine must continue for at least 740 s after the burst begins in this case.

Extended activity in the central engine can explain both of these flares. The central engine becomes active again around 150 and 300 s after the burst for XRF 050406 and GRB 050502B, respectively. The duration of the flare directly measures the duration of the central engine activity because the observed time sequence essentially follows the central engine time sequence (*19*).

With the exception of the flare at 213 s, the count rate of XRF 050406 was very low and detailed time-resolved spectroscopy is not possible. We can obtain some information on the spectral evolution of the flare, however, by dividing the data into two energy bands and examining light curves in those bands. Figure 2A shows the light curves in two bands (0.2 to 0.7 keV and 0.7 to 10 keV) bands, together with the ratio of these bands. There is significant spectral evolution during the first 400 s of this afterglow. During the rising flare (about $T + 180$ s to $T + 200$ s), the hard band flux spikes up rapidly while the soft band flux remains constant, indicating that the flare is harder spectrally than the underlying afterglow. Indeed, the rising portion of the flare contributes no notable flux between 0.2 and 0.7 keV, although it increases the count rate in the hard band by a factor of 4. This provides strong constraints on the flare mechanism: It is difficult to quadruple the flux in the high-energy band while the low-energy band remains constant, unless the flare is

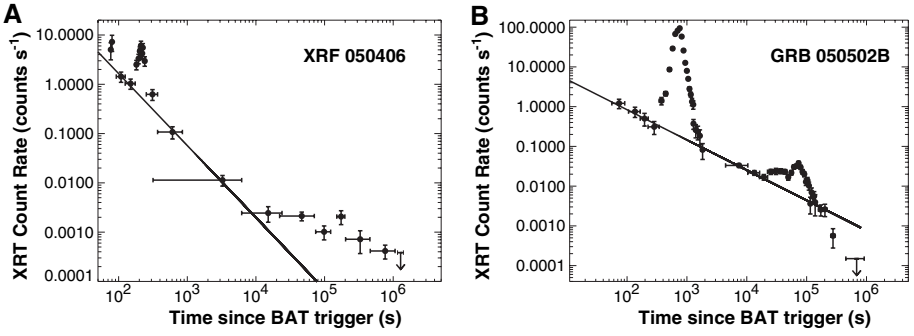

Fig. 1. Background-subtracted x-ray light curves of the afterglows of XRF 050406 (**A**) and GRB 050502B (**B**). Horizontal error bars show time bins; vertical error bars are means ± SD. For XRF 050406 we obtained a total exposure time of 155 ks distributed over 17 days; for GRB 050502B the total exposure time was 176 ks over 11 days. The solid lines represent power-law fits to the underlying afterglow decays from about 100 to 10,000 s [power-law index (±SD) is –1.5 ± 0.1 and –0.8 ± 0.2 for XRF 050406 and GRB 050502B, respectively]. The bright x-ray flares are superposed on this underlying power-law decay. At later times the XRF 050406 light curve flattens, whereas the GRB 050502B has several bumps, both suggesting late-time energy injection into the external shock or continued internal shock activity. The rapid decline in count rate for GRB 050502B at $T > 10^5$ s indicates a possible jet break at about 1 to 2 days postburst.

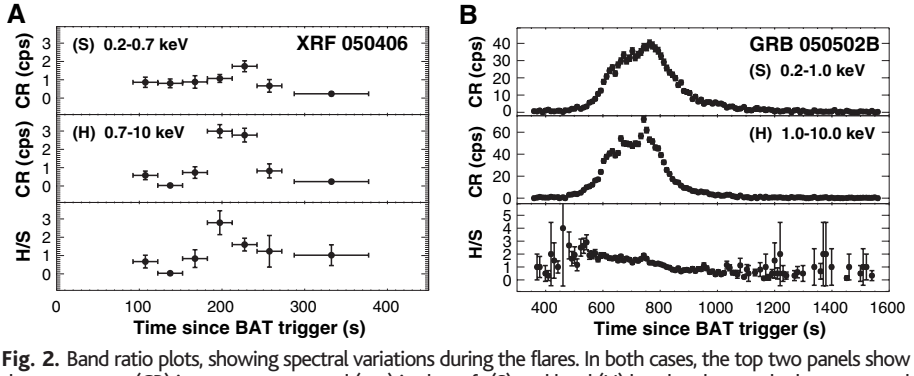

Fig. 2. Band ratio plots, showing spectral variations during the flares. In both cases, the top two panels show the count rates (CR) in counts per second (cps) in the soft (S) and hard (H) bands, whereas the bottom panel shows the band ratio (hard/soft). The boundaries between the hard and soft bands were chosen independently for each burst to provide comparable numbers of counts in the two bands. Horizontal error bars show time bins; vertical error bars are means ± SD. (**A**) Light curves in 0.2-to-0.7-keV and 0.7-to-10-keV bands for XRF 050406. The rising part of the flare is substantially harder than the decaying part of the flare or the underlying afterglow, suggesting that the flare is not caused by the external shock responsible for the underlying afterglow. (**B**) Light curves in 0.2-to-1.0-keV and 1-to-10-keV bands for GRB 050502B. The band ratio shows strong spectral variations during the large flare, with the ratio of counts in these bands decreasing by a factor of 4. The sharp spike in the hard band at about 740 s supports the internal shock interpretation for this flare, because such sharp features cannot easily be produced by external shocks.

strongly absorbed by a column of neutral gas $N_H \sim 10^{21}$ cm^{-2} that does not affect the underlying afterglow. However, the soft band peaks during the time bin following the overall peak, indicating that the emission softens substantially as the flare decays. If absorption is invoked for the rising portion of the flare, then the absorption seems to decrease markedly during the flare decay, suggesting that the absorbing gas may be ionized by the flare (*20*, *21*). After the flare, the band ratio returns to a value consistent with the preflare values. A band ratio plot of GRB 050502B also shows clear indications of spectral variations (Fig. 2B), with a trend similar to that in XRF 050406 (hardening at the beginning of the flare and gradually softening as the flare progresses), although in this case both bands increase during the rising portion of the flare.

We have referred to these events as x-ray flares because they were not detected by the higher energy BAT instrument on Swift. This is presumably due to the higher sensitivity of the XRT and to the steep spectral energy indices of the afterglows ($\beta = -1.3$ for the flare in XRF 050406 and $\beta = -1.4$ for the flare in GRB 050502B, where $F_x \propto E^{\beta}$). In the case of XRF 050406, the prompt emission was classified as an XRF because of its relatively soft spectrum. The discovery of these large x-ray flares in the afterglows raises the possibility that these flares themselves would be classified as XRFs had they not been preceded by the higher energy bursts detected by the BAT. Indeed, GRB 050502B appears to be a remarkable combination of a normal GRB followed more than 10 min later by an XRF of comparable fluence. [There is indirect evidence for a similar sequence in GRB 031203 (*22*)]. If a normal, relatively hard burst such as GRB 050502B can produce such a bright x-ray flare through late-time internal shocks, this suggests that XRFs themselves may be related to the characteristics of the central engine rather than to geometrical effects (*23*, *24*). However, the long durations and smooth temporal profile observed in these x-ray flares are quite different from those typically detected in XRFs (*25*).

Both of these afterglows appear to be dominated by long periods of energy production by the central engine, leading to a long period of x-ray emission from internal shocks extending long past the cessation of gamma-ray production. Such activity has previously been suggested as an explanation for extended GRB tails observed by the Burst and Transient Source Experiment (BATSE) instrument (*26*). In addition to the large flares several minutes after the burst, the plateaus or bumps beginning several hours later imply either that substantial energy is still being injected into the blast wave by refreshed shocks (*27*), that the external shocks are encountering dense clumps in the nearby interstellar medium (*28*), or that the internal shocks are still continuing up to several days after the burst in the observer's frame. The last possibility would require that the central engine operated for a time scale of days, possibly due to fallback of material into the central black hole (*29*, *30*).

If the central engine is still pumping substantial energy into the blast wave at such late times, how can one explain the short duration of the gamma-ray emission? The late internal shocks that produce the flares must produce lower energy photons than did the earlier internal shocks. This can be explained by higher bulk Lorentz factors, which result in lower magnetic fields at the larger radius reached by the internal shocks at these late times. For the internal shock model, the typical peak energy is $E_p \propto L^{1/2}R^{-1} \propto L^{1/2}\Gamma^{-2}\delta t^{-1}$ (*31*), where L is the luminosity at the flare epoch, R is the internal shock radius, Γ is the Lorentz factor, and δt is the variability time scale. If the flare occurs when R is 3 to 10 times larger than the typical internal shock radius of the burst, E_p may be 10 times lower. This is consistent with the detection of these flares in the x-ray band rather than in gamma-rays and with the large δt observed in the x-ray flares. The higher bulk Lorentz factors may arise because these late-time internal shocks benefit from a low-density channel through the progenitor star, previously excavated by the jets that produce the original gamma-ray burst. These later outflows would then have lower amounts of entrained baryons and higher Lorentz factors, leading to lower photon energies at later times and pushing the late-time internal shock emission below the BAT energy band (15 to 150 keV).

References and Notes

1. S. E. Woosley, *Astrophys. J.* **405**, 273 (1993).
2. A. I. MacFadyen, S. E. Woosley, *Astrophys. J.* **524**, 262 (1999).
3. J. Hjorth *et al.*, *Nature* **423**, 847 (2003).
4. K. Z. Stanek *et al.*, *Astrophys. J.* **591**, L17 (2003).
5. P. Mészáros, M. J. Rees, *Astrophys. J.* **476**, 232 (1997).
6. J. van Paradijs, C. Kouveliotou, R. A. M. J. Wijers, *Annu. Rev. Astron. Astrophys.* **38**, 379 (2000).
7. B. Zhang, P. Mészáros, *Int. J. Mod. Phys.* **19**, 2385 (2004).
8. N. Gehrels *et al.*, *Astrophys. J.* **611**, 1005 (2004).
9. D. N. Burrows *et al.*, *Space Sci. Rev.*, in press.
10. S. Barthelmy *et al.*, *Space Sci. Rev.*, in press.
11. D. N. Burrows *et al.*, *Astrophys. J.* **622**, L85 (2005).
12. S. Campana *et al.*, *Astrophys. J.* **625**, L23 (2005).
13. G. Tagliaferri *et al.*, *Nature* **436**, 985 (2005).
14. G. Cusumano *et al.*, in preparation.
15. Details of the burst properties are available as a supplementary table on *Science* Online.
16. L. Piro *et al.*, *Astrophys. J.* **623**, 314 (2005).
17. K. Ioka, S. Kobayashi, B. Zhang, *Astrophys. J.*, in press.
18. S. Kobayashi *et al.*, *Astrophys. J.*, in press.
19. S. Kobayashi, T. Piran, R. Sari, *Astrophys. J.* **490**, 92 (1997).
20. D. Lazatti, R. Perna, G. Ghisellini, *Mon. Not. R. Astron. Soc.* **325**, L19 (2001).
21. R. Perna, D. Lazzati, *Astrophys. J.* **580**, 261 (2002).
22. D. Watson *et al.*, in preparation.
23. E. Woods, A. Loeb, *Astrophys. J.* **523**, 187 (1999).
24. B. Zhang, X. Dai, N. M. Lloyd-Ronning, P. Mészáros, *Astrophys. J.* **601**, L119 (2004).
25. J. Heise, J. in't Zand, R. M. Kippen, P. M. Woods, in *Gamma-Ray Bursts in the Afterglow Era*, E. Costa, F. Frontera, J. Hjorth, Eds. (Springer, Berlin Heidelberg, 2001), pp. 16–21.
26. K. Hurley *et al.*, *Nature* **372**, 652 (1994).
27. M. J. Rees, P. Mészáros, *Astrophys. J.* **496**, L1 (1998).
28. D. Lazzati, E. Rossi, S. Covino, G. Ghisellini, D. Malesani, *Astron. Astrophys.* **396**, L5 (2002).
29. A. I. MacFadyen, S. E. Woosley, A. Heger, *Astrophys. J.* **550**, 410 (2001).
30. A. King *et al.*, *Astrophys. J. Lett.*, in press.
31. B. Zhang, P. Mészáros, *Astrophys. J.* **581**, 1236 (2002).

32. This letter is based on observations with the NASA Swift gamma-ray burst Explorer. We thank the Swift operations team for their support. The authors acknowledge support from NASA in the United States, ASI in Italy, and Particle Physics and Astronomy Research Council. in the UK.

Supporting Online Material

www.sciencemag.org/cgi/content/full/1116168/DC1
Table S1

15 June 2005; accepted 29 July 2005
Published online 18 August 2005;
10.1126/science.1116168
Include this information when citing this paper.

Molecular Octa-Uranium Rings with Alternating Nitride and Azide Bridges

William J. Evans,* Stosh A. Kozimor, Joseph W. Ziller

Uranium nitrides offer potential as future nuclear fuels and as probes of metal ligand multiple bonding involving the f-block actinide metals. However, few molecular examples are available for study owing to the difficulties in synthesis. Recent advances in organoactinide chemistry have provided a route to uranium nitride complexes that expands the options for developing UN chemistry. Several 24-membered uranium nitrogen rings, $(UNUN_3)_4$, have been synthesized by reduction of sodium azide with organometallic metallocene derivatives, $[(C_5Me_4R)_2U][(\mu\text{-}Ph)_2BPh_2]$ (R = Me, H; Me = methyl, Ph = phenyl). The nanometer-sized rings contain unusual UNU nitride linkages that have short U-N distances within the double-bond range.

Uranium nitrides have potential applications as future fuels in nuclear reactors owing to their high melting point, density, and thermal conductivity (*1*, *2*). Attachment of nitride ions, N^{3-}, to uranium is also of interest with respect to the nature of multiple bonding when